Supporting information for

Decoupling proton-electron transfer facilitates the OER kinetics on Ru-Pb binary electrocatalyst

Rui Huang[1]†, Yunzhou Wen[1]†, Huisheng Peng[1] and Bo Zhang[1]*

[1]*State Key Laboratory of Molecular Engineering of Polymers, Department of Macromolecular Science and Laboratory of Advanced Materials, Fudan University, Shanghai 200438, China.*

†These authors contributed equally to this work.

**Correspondence and requests for materials should be addressed to Bo Zhang (bozhang@fudan.edu.cn) (B.Z.).*

Experimental section

Detailed electrochemical measurements. For electrochemical measurements on CPs, the catalysts were sprayed onto CPs using an airbrush. 20 mg catalysts were first dispersed in 2 mL isopropanol, and then 80 μL of 5 wt. % Nafion® solution was added. After at least 60 min sonication, the homogeneous ink was sprayed onto 2 cm × 2 cm CP heated to 80°C. The CPs were weighed before and after airbrush and the total catalyst loading was controlled at *ca.* 1.5 mg cm^{-2}.

To assess the OER catalytic activity, the working electrode was first scanned from 0.3 to 0.9 V *vs.* Hg/Hg_2SO_4 at a rate of 100 mV s^{-1} for 10 cycles to achieve stable cyclic voltammetry (CV) scans in 0.5 M H_2SO_4 (pH=0.10). The pH of the solution was measured by a Horiba D-71 pH meter before each experiment. Then linear sweep voltammetry (LSV) was measured at 5 mV s^{-1} under 2,500 rpm rotation. All measurements were conducted at room temperature. All potentials were referred to the reversible hydrogen electrode (RHE) by the following calculations:

$$E_{\mathrm{RHE}} = E_{\mathrm{Hg/Hg_2SO_4}} + 0.652 + 0.0591 \times \mathrm{pH}$$

All the potentials were applied a 95% iR compensation. The uncompensated solution resistances were measured by electrochemical impedance spectra (EIS), which were conducted at a bias of 1.40 V, 1.42 V and 1.45 V *vs.* RHE in the frequency range from 100 kHz to 50 mHz with an amplitude of 10 mV. For the pH-dependence measurements, the 0.05M, 0.1M, 0.25M and 0.5M H_2SO_4 solutions were used without adding any buffers. The average pH of the solutions was 1.06, 0.80, 0.39 and 0.20, respectively. The average uncompensated solution resistances used in iR-correction were 62 Ω, 33 Ω, 14 Ω, and 8 Ω for different pH.

The steady-state Tafel plots were measured by chronoamperometry on rotation disk electrodes (2,500 rpm). The sample was held at constant potential from 1.25 V to 1.75V *vs.* RHE with a step of 20 mV. Each potential step was retained for 10 s to reach stable and the final current was recorded.

ECSA was deduced from electrochemical double-layer capacitance (C_{dl}) by dividing a factor of 0.035 mF cm^{-2}, according to the previous report [1]. The measurement of C_{dl} was carried out by cyclic voltammetry (CV) at the non-Faradic region or fit from EIS spectra (see Supplementary Note 1). The catalysts were scanned at a range of +0.20 to +0.30 V *vs.* Hg/Hg_2SO_4 using elevated scan rates. Both anodic and cathodic current at +0.25 V *vs.* Hg/Hg_2SO_4 were plotted against scan rates. Then, linear fitting was adopted to these points, and the average slope of anodic and cathodic plots represented the value of C_{dl}.

To eliminate the interference of bubble accumulation and mechanical peeling of catalysts, the OER stability was evaluated on carbon paper by chronopotentiometry at 10 mA cm^{-2}_{geo}. The electrochemical cell was placed in a 25 ^{o}C thermostatic water bath. The v-t plots were 95% iR-compensated.

The pulse voltammetry was measured according to the protocols reported by Nong *et al.* [2] The potential was kept at a low potential (E_{low} = 1.32 V) for 4 s, then switched and kept at a higher potential (E_{high}) for 5 s before returning to E_{low} for 4 s. This cycle was repeated while increasing E_{high} from 1.34 V to 1.70 V in 20 mV per step and keep E_{low} unchanged. The charge stored in the catalyst was calculated by integrating the cathodic pulse current.

X-ray absorption spectroscopy. Ru K-edge XAFS measurements were performed in fluorescent mode at 1W1B beamline in Beijing Synchrotron Radiation Facility (BSRF). The absorption energy (E_0) of Ru K-edge was calibrated to 22117 eV by metallic Ru powder. All XAFS data were processed and normalized by ATHENA software included in IFEFFIT software package [3]. As to the fitting and simulation of EXAFS data, the ARTEMIS software and FEFF8.5 codes were used. The detailed discussion of EXAFS fitting is presented in Supplementary note 2.

PEM electrolyzer test. A catalyst-coated membrane (CCM) method was used to prepare the anode layer of the membrane electrode assembly (MEA). The anode catalyst was first dispersed in a mixture of isopropanol and Nafion® solution, and the ionomer amount was 20 wt. %. After adequate sonication, the homogeneous inks were sprayed onto a piece of 50 μm polytetrafluoroethylene (PTFE) film. The CCM was obtained by transferring the catalyst layer from the PTFE film to a Nafion® NR212 membrane using the decal method (140^{o}C, 10 Mpa for 2 min). The CCM was then boiled in 0.5 M H_2SO_4 and DI water to remove impurities. For the cathode, a catalyst-coated diffusion layer was used. 40% Pt/C was used as a cathodic catalyst and sprayed onto a Freudenberg H23C9 gas diffusion layer. The ionomer amount in the cathode was 30 wt. %. The mass loadings were controlled at 1 mg_{cat} cm^{-2} and 0.2 mg_{Pt} cm^{-2} for anodic and cathodic catalysts, respectively. A porous Ti paper was used as a porous transport layer (PTL) for the anode. Finally, the cell was integrated by pressing cathodic diffusion layer, CCM, PTL and two Ti end-plates with flow field together. The active area was 5 cm^2l. During the test, the cell was maintained at 80^{o}C, and the pre-heated DI water was fed to the anode at a flow rate of 40 ml min^{-1}. The steady-state polarization curve was collected at potentiostat mode from 1 V to 2 V. Each step was 50 mV and maintained for 30 s until the current was stable.

Supplementary Notes

Supplementary Note 1: Evaluation of intrinsic activities

The intrinsic activities of different catalysts can be evaluated by calculation turnover frequency (TOF) or by normalizing the OER current by electrochemical surface area (ECSA).

TOF is defined as the frequency of reaction per active site, which is used to compare the intrinsic activity of different catalysts. TOF value in this study was calculated by the equation:

$$\mathrm{TOF} = \frac{j \times A \times \eta}{4 \times e \times n}$$

where j is the current density after 95% iR compensation, A is the geometric area of GCE (0.0706 cm^2), η is the Faradic efficiency (assumed as 100%) and e is the charge of an electron (1.602×10^{-19} C) and n is the number of active sites.

We determined the active site number n *via* the total loading mass by assuming all Ru atoms as active sites (underestimating case), according to the following equation:

$$n_{\mathrm{mass}} = \frac{m_{\mathrm{loading}} \times \mathrm{N_A}}{\mathrm{Mw}} \times n_{\mathrm{Ru}}$$

where m_{loading} is the loading mass. $\mathrm{N_A}$ is Avogadro's constant (6.022×10^{23} mol^{-1}), Mw is the molecular weight of catalysts and n_{Ru} is the number of Ru atoms per molar of catalysts. The Mw of $RuPbO_x$ is estimated as 904.7 g mol^{-1} ($Ru_5Pb_1O_{12}$).

ECSA was deduced from electrochemical double-layer capacitance (C_{dl}) by dividing a factor of 0.035 mF cm^{-2}, according to the previous report [1]. In this work, the measurement of C_{dl} was carried out by two different methods: (i) cyclic voltammetry (CV) at the non-Faradic region and (ii) fit from EIS Nyquist plots.

For measuring C_{dl} in the non-Faradic region, the catalyst-loaded GCEs were scanned at a range of +0.2 to +0.3 V *vs.* Hg/Hg_2SO_4 using elevated scan rates. Both anodic and cathodic current at +0.25 V *vs.* Hg/Hg_2SO_4 were plotted against scan rates (Supplementary Figure 5). Then, linear fitting was adopted to these points, and the average slope of anodic and cathodic plots represented the value of C_{dl}.

For the fittings from EIS method is that it is an *in-situ* measurement, an R(RQ)(RQ) equivalent circuit was used in the fit. Q is the constant phase element (CPE). R_s is the uncompensated solution resistance. The parallel of R_{film} and CPE1 refers to the dielectric properties of the catalyst film [4], while the parallel of R_{ct} and CPE2 represents the interfacial charge transfer resistance and the double-layer capacitance (C_{dl}). The effective $C_{dl,eff}$ was deduced according to the following equation [2, 5]:

$$C_{dl,eff} = Q_2^{\frac{1}{\alpha_2}}\left(\frac{1}{R_s} + \frac{1}{R_{film} + R_{ct}}\right)^{\frac{\alpha_2 - 1}{\alpha_2}}$$

where Q_2 is a constant with units of mho $s^{\alpha-1}$, and $0\leq\alpha\leq1$ is related to the phase angle of the frequency response. The fitting result and corresponding parameters are presented in Supplementary Figure 9 and Supplementary Table 4.

BET surface area is also used to estimate the intrinsic activity in this work. For aggregated nanoparticles, as was in our case, the BET surface area could also reflect the actual electrochemical surface area to some extent.

Supplementary Note 2: XAS measurements and analysis

For Ru K-edge data, the absorption edge energy E_0 of pure Ru foil was aligned to 22117 eV. E_0 of Ru foil was assigned by the first maximum of the first-derivative X-ray absorption near-edge structures (XANES) spectrum. All data were aligned according to the standard Ru foil.

The simulation of the EXAFS spectra of $RuPbO_x$ was carried out by the FEFF 8.5 codes embedded in the *Artemis* software. The crystallographic information file (CIF) of RuO_2, was used as the primary model to

calculate raw scattering paths [6]. Ru-Pb scattering paths were created by replacing corresponding Ru atoms in the FEFF input file. The experimental spectra were fitted by raw scattering paths at a k-range of 3.5 to 13 $Å^{-1}$.

We adopted the following criteria during the fits to rationalize the process:

(i) The passive electron reduction factor S_0^2 was set as the same for all paths;

(ii) For each element, the same energy shifts (E_0) were used;

(iii) For each element, the same squared displacement σ_i^2 was used;

(iv) The degeneracy of second shell O and Ru was fixed at 4 and 2, respectively.

Supplementary Figures

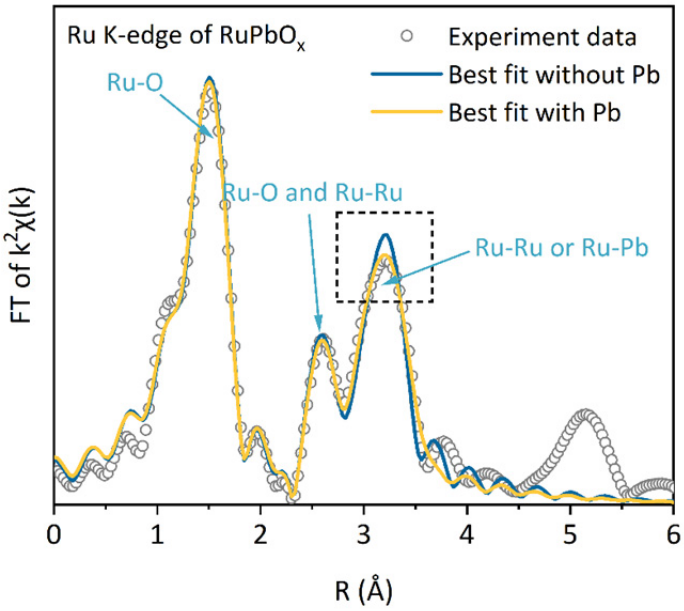

Supplementary Figure 1 | Fitting of Ru K-edge EXAFS data. A better fit was obtained when the Ru-Pb scattering path was included, indicating the Pb atoms were doped into rutile lattice at the atomic scale.

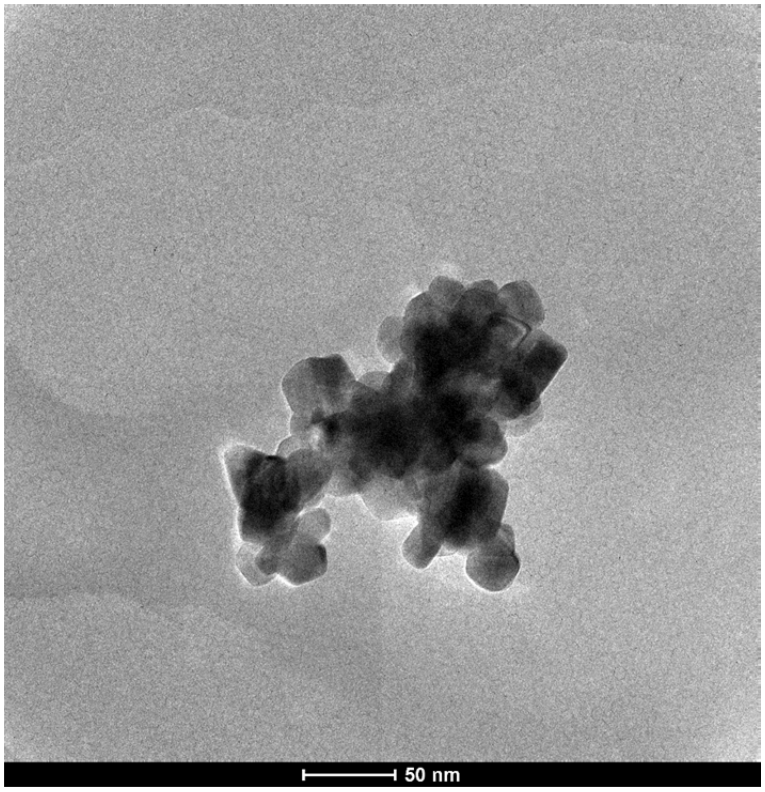

Supplementary Figure 2 | TEM image of commercial RuO_2. The catalysts are ~20 nm nanoparticles, similar to $RuPbO_x$ in size.

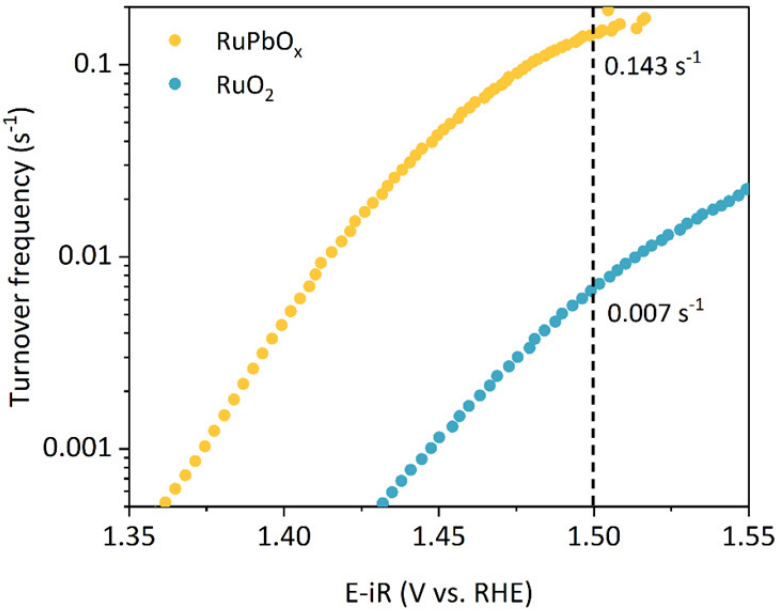

Supplementary Figure 3 | TOF of different catalysts.

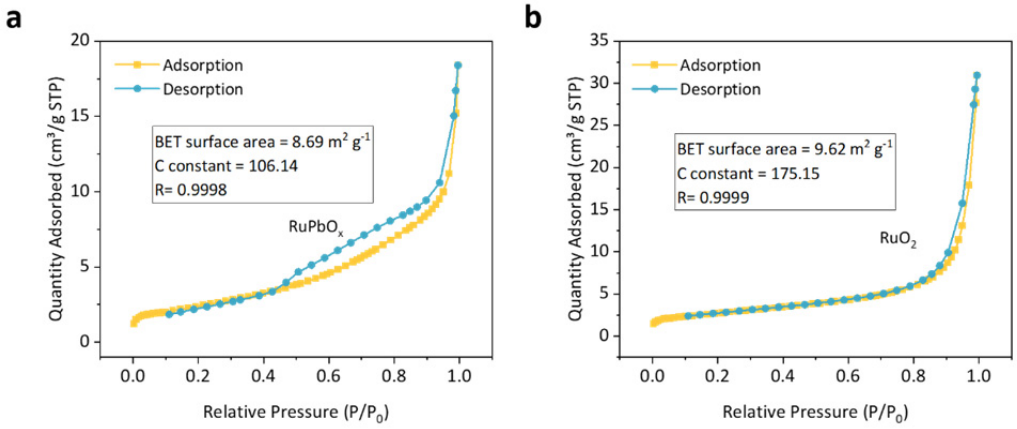

Supplementary Figure 4 | BET isotherm plots of (a) $RuPbO_x$ and (b) RuO_2.

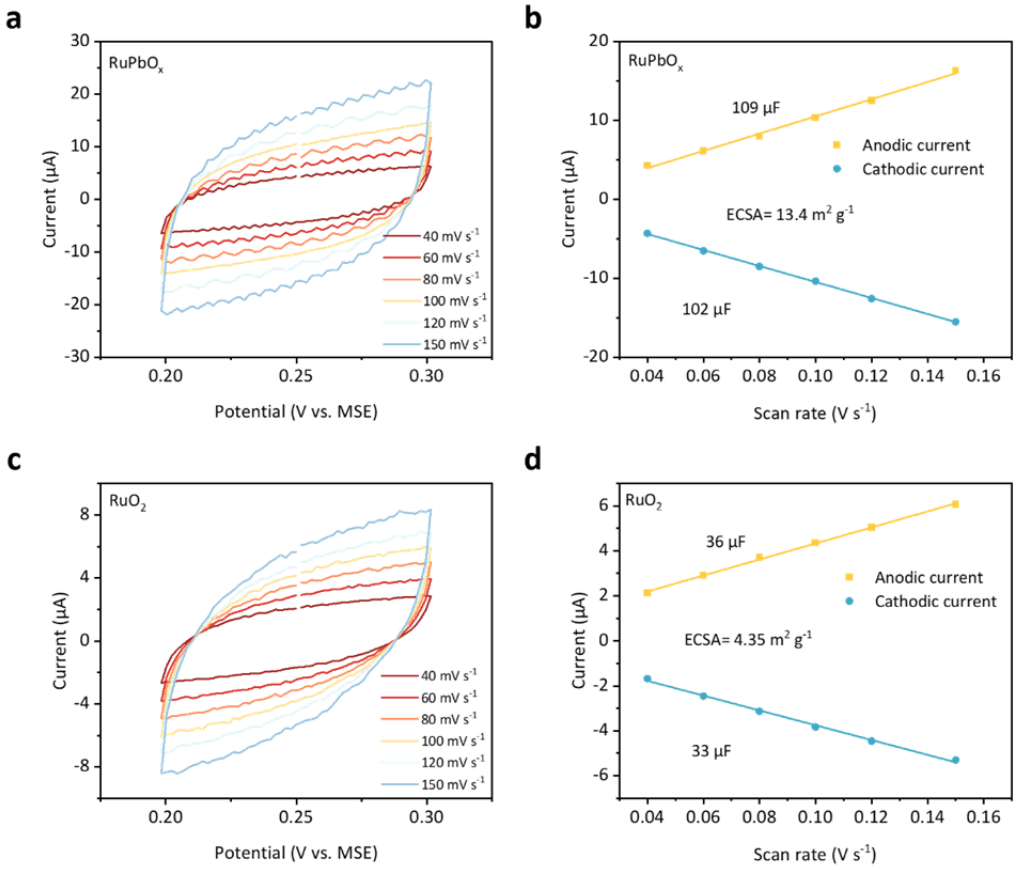

Supplementary Figure 5 | ECSA of $RuPbO_x$ and RuO_2. (a-b) $RuPbO_x$. **(c-d)** RuO_2. The ECSA values were obtained from the double-layer capacitance (C_{dl}) at the non-Faradic region. The C_{dl} was measured by CV scans at elevated scan rates.

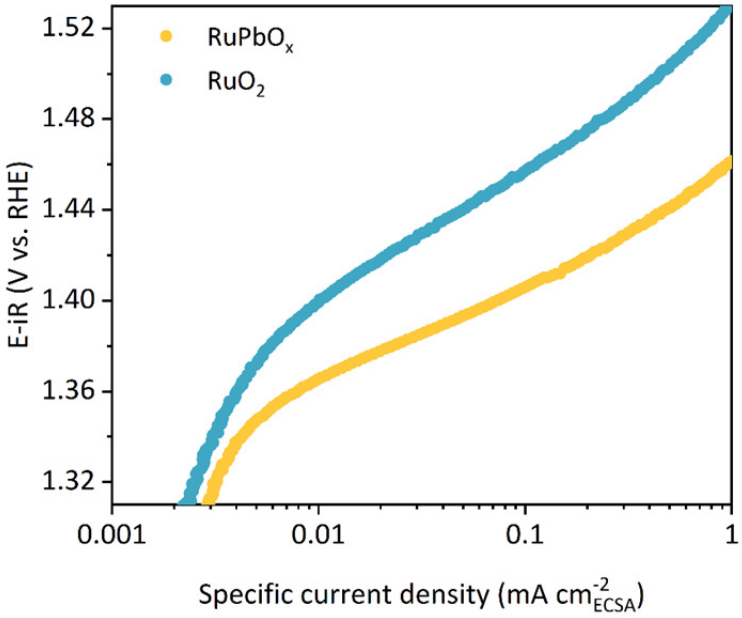

Supplementary Figure 6 | OER polarization curves normalized using ECSA.

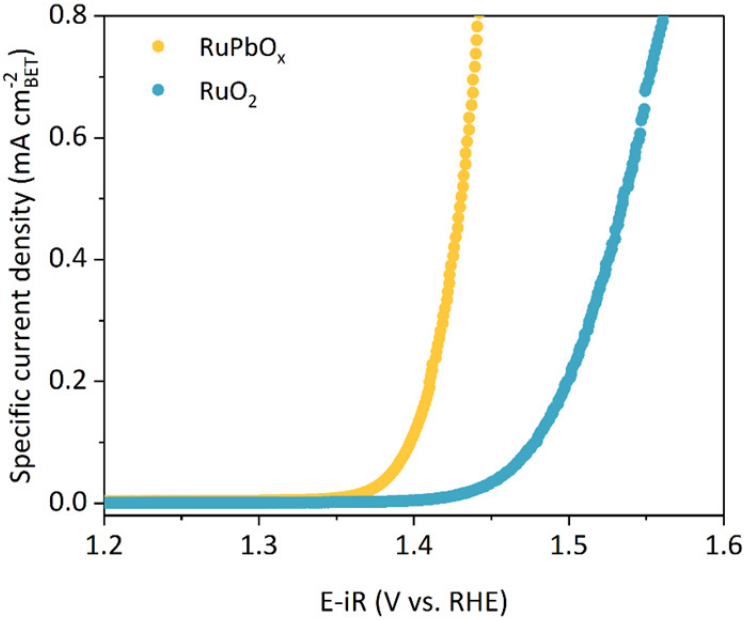

Supplementary Figure 7 | OER polarization curves normalized using BET surface area.

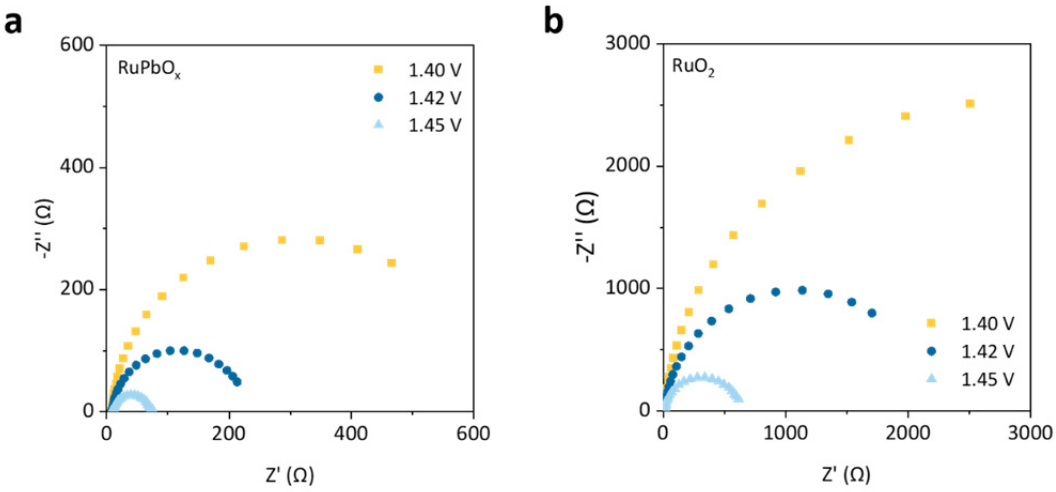

Supplementary Figure 8 | EIS of $RuPbO_x$ and RuO_2 at different potentials. (a) $RuPbO_x$. **(b)** RuO_2.

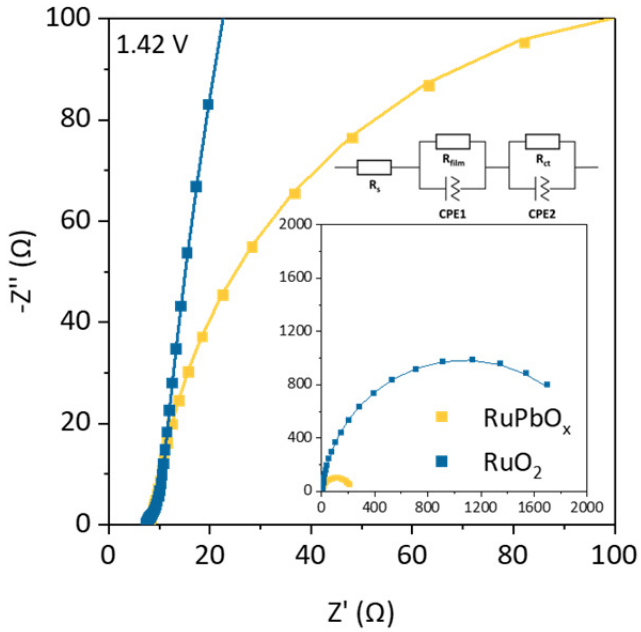

Supplementary Figure 9 | Fitting of EIS spectra at 1.42 V *vs*. RHE. An R(RQ)(RQ) equivalent circuit was used in the fit. Q is the constant phase element (CPE). R_s is the uncompensated solution resistance. The parallel of R_{film} and CPE1 refers to the dielectric properties of the catalyst film, while the parallel of R_{ct} and CPE2 represents the interfacial charge transfer resistance and the double-layer capacitance (C_{dl}). The fitting results are summarized in **Supplementary Table 4**.

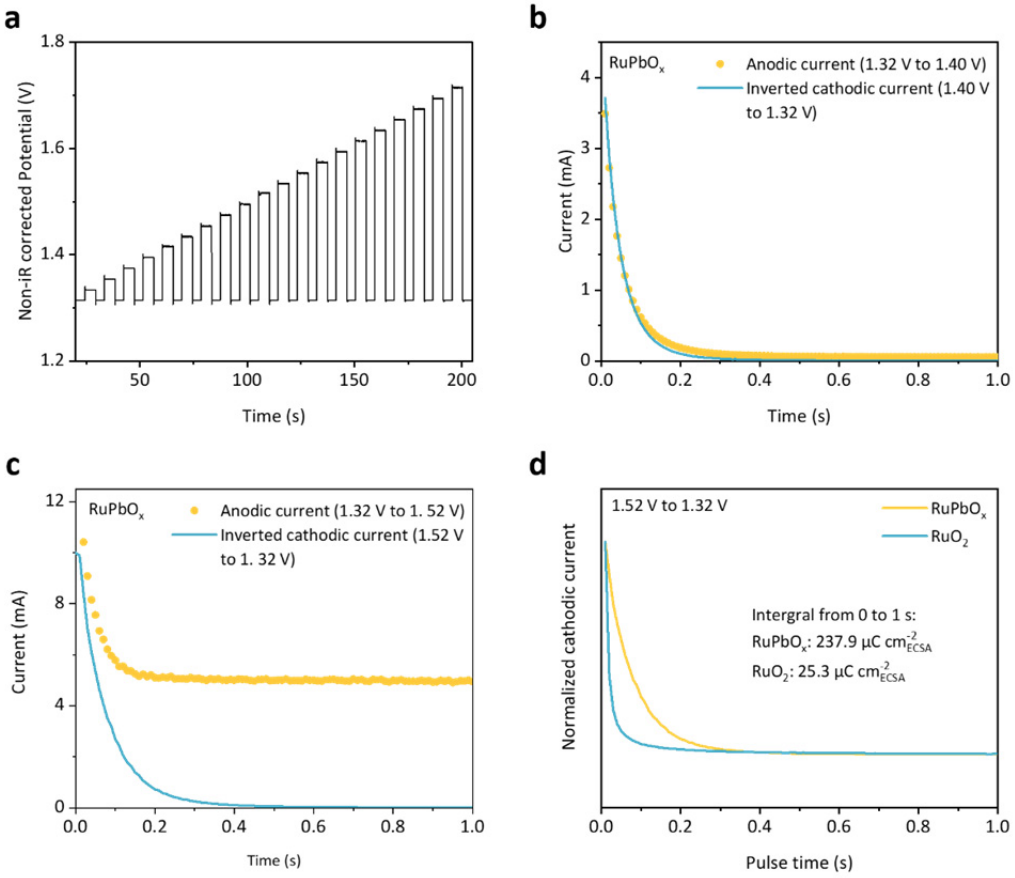

Supplementary Figure 10 | The measurements of charge storage profiles using pulse voltammetry. The details of pulse voltammetry are referred to in ref. [2]. **(a)** Pulse voltammetry protocol between 1.32 V cathodic and 1.34 V to 1.72 V anodic non-iR corrected potentials. **(b)** Anodic (1.32 V to 1.40 V) and inverted cathodic current (1.40 V to 1.32 V) decay of $RuPbO_x$ when no OER take place. **(c)** Anodic (1.32 V to 1.52 V) and inverted cathodic current (1.52 V to 1.32 V) decay of $RuPbO_x$ when OER take place. **(d)** The cathodic current relaxation time of $RuPbO_x$ is longer than RuO_2, indicating more charge stored in the $RuPbO_x$ surface. The charge stored in catalysts are calculated by integrating the cathodic pulse current.

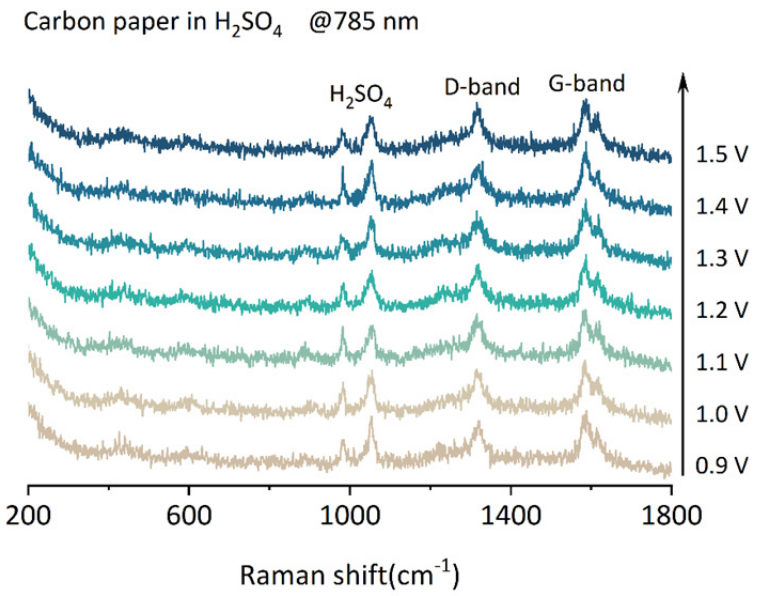

Supplementary Figure 11 | EC-Raman spectra of empty carbon paper in the H_2SO_4. The peak at 980 cm^{-1} and 1052 cm^{-1} came from H_2SO_4 in the electrolyte. The 1320 cm^{-1} and 1586 cm^{-1} are D-band and G-band from carbon paper.

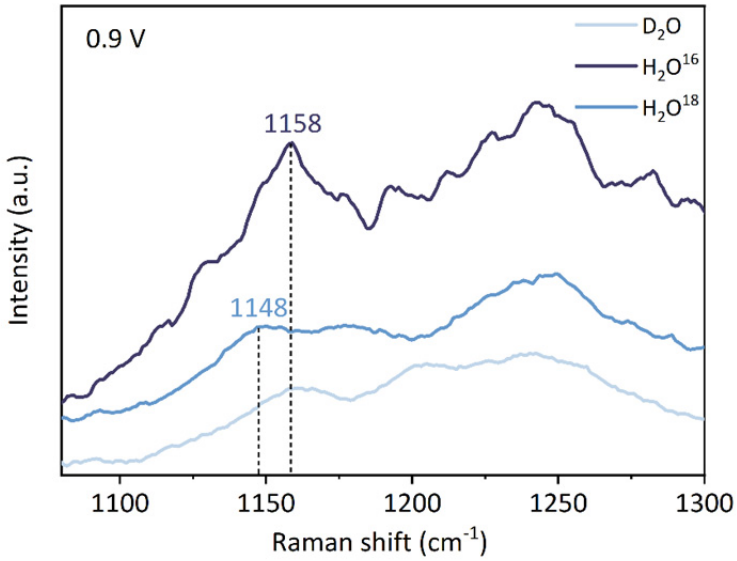

Supplementary Figure 12 | EC-Raman spectra of $RuPbO_x$ in the wavenumber region 1100-1300 cm^{-1}. The spectra were obtained at 0.9 V *vs*. RHE in 0.5 M H_2SO_4, D_2SO_4 and $H_2S^{18}O_4$, respectively.

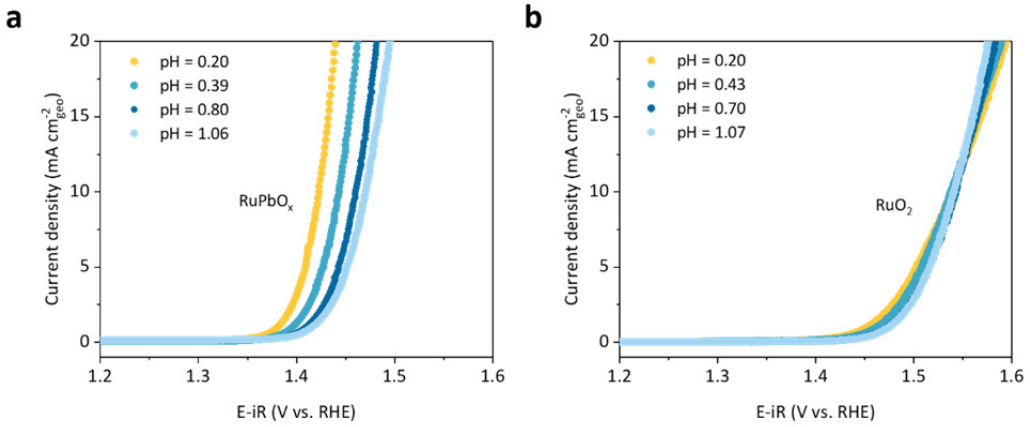

Supplementary Figure 13 | LSV curves of $RuPbO_x$ and RuO_2 measured in different pH. Scan rate: 5 mV s^{-1}.

Supplementary Tables

Supplementary Table 1 | Parameters used in the Ru K-edge EXAFS fitting of $RuPbO_x$.

Fit	Path	CN	S_0^2	σ^2	E_0	R (Å)
With Ru-Pb scattering path	Ru-O 1#	5.80±0.40	0.85	0.0029	0.134	1.977±0.003
	Ru-Ru 1#	2 (set)	0.85	0.0040	-7.988	3.079±0.019
	Ru-O 2#	4 (set)	0.85	0.0029	0.134	3.457±0.090
	Ru-Ru 2#	5.48±0.62	0.85	0.0040	-7.988	3.526±0.006
	Ru-Pb	2.93±2.00	0.85	0.0053	12.624	3.485±0.018
Without Ru-Pb scattering path	Ru-O 1#	5.60±0.62	0.85	0.0028	-0.151	1.982±0.007
	Ru-Ru 1#	2 (set)	0.85	0.0034	-6.053	3.095±0.010
	Ru-O 2#	4 (set)	0.85	0.0028	-0.151	3.412±0.047
	Ru-Ru 2#	5.49±0.73	0.85	0.0034	-6.053	3.547±0.010

Supplementary Table 2 | Summary of electrochemical performance of different samples on GCE.

Catalyst	Onset potential[1] (mV)	Overpotential[2] (mV)	Tafel slope (mV dec^{-1})
$Ru_3Pb_1O_x$	169±2	221±4	45
$Ru_5Pb_1O_x$	151±1	191±3	39
$Ru_7Pb_1O_x$	171±3	218±2	44
RuO_2	211±10	285±3	63

[1] Overpotential at 1 mA cm^{-2}.

[2] Overpotential at 10 mA cm^{-2}.

Supplementary Table 3 | Performance summary of previous reported OER catalysts in acidic environment.

Catalyst	η^2	Mass activity	Tafel slope	Stability	Reference
$RuPbO_x$	**191±3 mV**	**593 A g_{Ru}^{-1} @ 270 mV**	**39 mV dec^{-1}**	**100h @ 10 mA cm^{-2}**	**This work**
RuO_2	**285±3 mV**	**28 A g_{Ru}^{-1} @ 270 mV**	**63 mV dec^{-1}**	**-**	**This work**
Li-IrO_x	270 mV	1000 A g_{Ir}^{-1} @ 345 mV	39 mV dec^{-1}	10h @ 10 mA cm^{-2}	Ref.[7]
$RuIrO_x$ nano-netcage	233 mV		42 mV dec^{-1}	24h @ 1.45V (full cell)	Ref.[8]
$Cr_{0.6}Ru_{0.4}O_2$ (550)	178 mV	229 A g_{cat}^{-1} @ 270 mV	56-58 mV dec^{-1}	10h @ 10 mA cm^{-2}	Ref.[9]
Ru@IrO_x	282 mV	645 A g_{cat}^{-1} @ 330 mV	69.1 mV dec^{-1}	24h @ 1.55V *vs*. RHE	Ref.[10]
Co-RuIr	235 mV		66.9 mV dec^{-1}	25h @ 10 mA cm^{-2}	Ref.[11]
Ru_1–PtCu	220 mV	779 A g_{metal}^{-1} @ 280 mV		28h @ 10 mA cm^{-2}	Ref.[12]
Pd@Ru	257 mV		63 mV dec^{-1}	10h @ 1.45V *vs*. RHE	Ref.[13]

Cu-doped RuO_2	188 mV	44 mV dec^{-1}	8h @ 10 mA cm^{-2}	Ref.[14]
$Y_2Ru_2O_{7-\delta}$	190 mV (onset)	46-55 mV dec^{-1}	8h @ 1 mA cm^{-2}	Ref.[15]

[1] Overpotential at 10 mA cm^{-2}.

Supplementary Table 4 | Summary of parameters used in EIS fittings on GCE.

Parameters	$RuPbO_x$	RuO_2
R_s (Ω)	7.96	7.56
R_{film} (Ω)	2.07	2.71
CPE1.Q_1 (mMho $s^{\alpha-1}$)	15.2	1.92
CPE1.α_1	0.74	0.76
R_{ct} (Ω)	213	2126
CPE2.Q_2 (mMho $s^{\alpha-1}$)	3.46	0.69
CPE2.α_2	0.97	0.95
$C_{dl,eff}$ (mF)	3.14	0.53
ECSA[1] (m^2 g^{-1})	399	67

[1] Derived by dividing a roughness factor of 0.035 mF cm^{-2}.

Supplementary Table 5 | The deconvolution of O 1s XPS spectra using CasaXPS software.

Sample	Peak	Lineshape	Position (eV)	FWHM	Area
$RuPbO_x$	lattice O	LA(1.53,243)	528.77	1.02	3010.42
	ads. OH	LA(1.53,243)	531.42	2.83	28527.32
	ads. H_2O	LA(1.53,243)	534.23	2.43	19649.30
RuO_2	lattice O	LA(1.53,243)	528.74	0.90	22680.26
	ads. OH	LA(1.53,243)	530.42	2.78	51041.21
	ads. H_2O	LA(1.53,243)	533.10	4.15	24324.04

References

[1] C. C. McCrory, S. Jung, J. C. Peters, T. F. Jaramillo, *J. Am. Chem. Soc.* **2013**, 135, 16977-16987.

[2] H. N. Nong, L. J. Falling, A. Bergmann, M. Klingenhof, H. P. Tran, C. Spori, R. Mom, J. Timoshenko, G. Zichittella, A. Knop-Gericke, S. Piccinin, J. Perez-Ramirez, B. R. Cuenya, R. Schlogl, P. Strasser, D. Teschner, T. E. Jones, *Nature* **2020**, 587, 408-413.

[3] B. Ravel, M. Newville, *J. Synchrotron Rad.* **2005**, 12, 537-541.

[4] M. E. Orazem, I. Frateur, B. Tribollet, V. Vivier, S. Marcelin, N. Pébère, A. L. Bunge, E. A. White, D. P. Riemer, M. Musiani, *J. Electrochem. Soc.* **2013**, 160, C215-C225.

[5] G. Li, L. Anderson, Y. Chen, M. Pan, P.-Y. Abel Chuang, *Sustainable Energy & Fuels* **2018**, 2, 237-251.

[6] C.-E. Boman, J. Danielsen, A. Haaland, B. Jerslev, C. E. Schäffer, E. Sunde, N. A. Sørensen, *Acta Chem. Scand.* **1970**, 24, 116-122.

[7] J. Gao, C. Q. Xu, S. F. Hung, W. Liu, W. Cai, Z. Zeng, C. Jia, H. M. Chen, H. Xiao, J. Li, Y. Huang, B. Liu, *J. Am. Chem. Soc.* **2019**, 141, 3014-3023.

[8] Z. Zhuang, Y. Wang, C. Q. Xu, S. Liu, C. Chen, Q. Peng, Z. Zhuang, H. Xiao, Y. Pan, S. Lu, R. Yu, W. C. Cheong, X. Cao, K. Wu, K. Sun, Y. Wang, D. Wang, J. Li, Y. Li, *Nat. Commun.* **2019**, 10, 4875.

[9] Y. Lin, Z. Tian, L. Zhang, J. Ma, Z. Jiang, B. J. Deibert, R. Ge, L. Chen, *Nat. Commun.* **2019**, 10, 162.

[10] J. Shan, C. Guo, Y. Zhu, S. Chen, L. Song, M. Jaroniec, Y. Zheng, S.-Z. Qiao, *Chem* **2019**, 5, 445-459.

[11] J. Shan, T. Ling, K. Davey, Y. Zheng, S. Z. Qiao, *Adv. Mater.* **2019**, 31, e1900510.

[12] Y. Yao, S. Hu, W. Chen, Z.-Q. Huang, W. Wei, T. Yao, R. Liu, K. Zang, X. Wang, G. Wu, W. Yuan, T. Yuan, B. Zhu, W. Liu, Z. Li, D. He, Z. Xue, Y. Wang, X. Zheng, J. Dong, C.-R. Chang, Y. Chen, X. Hong, J. Luo, S. Wei, W.-X. Li, P. Strasser, Y. Wu, Y. Li, *Nat. Catal.* **2019**, 2, 304-313.

[13] Y. Hu, X. Luo, G. Wu, T. Chao, Z. Li, Y. Qu, H. Li, Y. Wu, B. Jiang, X. Hong, *ACS Appl. Mater. Interfaces* **2019**, 11, 42298-42304.

[14] J. Su, R. Ge, K. Jiang, Y. Dong, F. Hao, Z. Tian, G. Chen, L. Chen, *Adv. Mater.* **2018**, e1801351.

[15] J. Kim, P. C. Shih, K. C. Tsao, Y. T. Pan, X. Yin, C. J. Sun, H. Yang, *J. Am. Chem. Soc.* **2017**, 139, 12076-12083.